Effect of external electromagnetic radiation on the anomalous metallic behavior in superconducting Ta thin films

Junghyun Shin, Sungyu Park,* and Eunseong Kim†
Department of Physics, KAIST, Daejeon 34141, Republic of Korea

(Received 23 July 2020; revised 7 October 2020; accepted 7 October 2020; published 3 November 2020)

We investigated the transport characteristics of superconducting Ta thin films with three configurations of radio-frequency radiation filters: no filter, only room-temperature filter, and low- and room-temperature filters. We find that when the room-temperature filter is installed, the entire transition is shifted to higher temperatures, and once the zero-resistance state is achieved at zero magnetic field, no strong radiation effect is observed. When the magnetic field is turned on, the non-zero-resistance saturation at low temperatures is revealed without low-temperature filters, which has previously been considered to be a magnetic-field-induced quantum metallic phase. However, the insertion of the additional low-temperature filters weakens the saturation of the resistance, i.e., the signature of the metallic behavior. This observation suggests that the previously reported anomalous metallic state in Ta films is mainly induced by unfiltered radiation, and, thus, the intrinsic metallic ground state, if it exists, should be limited to a narrow range of magnetic fields near the critical point.

DOI: 10.1103/PhysRevB.102.184501

I. INTRODUCTION

The scaling theory of localization anticipates that the ground state of two-dimensional (2D) noninteracting electron systems is an insulating state because intrinsic disorders prohibit the appearance of a metallic state [1]. Strong correlation of electrons, which allows the appearance of superconductivity, can be marginally observed in 2D superconductors because of their susceptibility to external perturbations, such as disorders, currents, and magnetic fields (B). Accordingly, the direct superconductor-insulator (SI) transition was theoretically proposed with a metallic ground state considered to exist only at the boundary between the two phases [2,3].

The SI transition has been investigated experimentally with various approaches. For instance, finite-size scaling analysis [4] near the quantum critical point has been utilized to examine the universal features of the SI transition [2,5]. Temperature (T) dependence of resistance at low temperatures has been investigated to examine the ground state of disordered films [6]. Otherwise, AC conductance [7], scanning tunneling microscopy [8], and Nernst effect measurements [9] have been conducted to identify the nature of the SI transition.

Nevertheless, an anomalous metallic phase at the zero-temperature limit has been observed. The magnetic-field-tuned metallic state was first observed in a study of amorphous MoGe thin films [10]; under a wide range of magnetic fields, decreasing resistance with thermally activated behavior at relatively high temperatures transformed into temperature-independent finite resistance saturation at low temperatures. This metallic behavior has since been widely reported in various thin films, such as highly disordered InOx films [11] and weakly disordered Ta films [12], as well as 2D crystalline films of both 2H-$NbSe_2$ [13] and ion-gated ZrNCl [14].

The apparent metallic behavior at low temperatures has been interpreted as the appearance of a Bose metal [15] and dissipation induced by quantum tunneling [16]. However, these interpretations have been challenged by the fact that unfiltered electromagnetic radiation can elevate electron temperature, which may disrupt the phase coherence in superconductivity. Skepticism has intensified by the recent observation of a strong suppression of the metallic behavior by an adequate filtering of radiation [17] where the installation of several layers of electromagnetic radiation filters substantially reduced the resistance saturation in both 2H-$NbSe_2$ and highly disordered InOx films. On the other hand, a more recent transport study on YBCO thin films patterned with a triangular array of holes reported the existence of Cooper-pair phase coherence with finite-resistance saturation at low temperatures with an adequately filtered measurement architecture [18,19]. Thus, the physical origin of the unexpected metallic behavior still remains controversial.

Ta thin films [12,20–22], a weakly disordered 2D superconducting system, such as MoGe thin films [10,23,24], show distinct characteristics that are clearly separated from ideal disorder-free crystalline 2H-$NbSe_2$ and strongly disordered InOx films. The 2H-$NbSe_2$ [25,26] films exhibit superconductivity even in the monolayer limit and quantum Griffiths singularity whereas revealing similar transport characteristics as weakly disordered superconducting thin films: fragile dissipationless states over a wide range of magnetic fields. On the other hand, InOx films show a significant magnetoresistance peak [27–29] and an extremely weak intermediated metallic phase in a narrow magnetic-field range [17]. Thus, disorder strength plays a key role in determining transport

*Present address: Center for Artificial Low Dimensional Electronic Systems, Institute for Basic Science (IBS), Pohang 37673, Republic of Korea.
†eunseong@kaist.edu

TABLE I. List of superconducting Ta films.

Sample	Batch	d(nm)	$R_N(k\Omega)$	$T_C(K)$
Ta1-1	1	3.8	2.49	0.27
Ta1-2	1	4.0	1.89	0.32
Ta1-3	1	5.0	1.54	0.44
Ta2-1	2	4.0	1.17	0.43

characteristics in the SI transition. Distinct from 2H-$NbSe_2$ films, both Ta and InOx films have a disordered amorphous structure. The surface roughness of Ta thin films [22] is much smoother than that of InOx films [11,30]; such discrepancies in surface morphology lead to dramatic differences in the level of disorder. In this paper, we present the effects of radiation filtering on the transport characteristics of representative weakly disordered Ta thin films in addition to those of highly disordered InOx and disorder-free $NbSe_2$ [17]. The introduction of a layered filtering architecture vastly reduces the dissipation below the transition temperature (T_C), and accordingly, the metallic behavior. A phase diagram on the B-T plane directly exhibits the suppression of the metallic phase, which intervenes between the superconducting and the insulating phases.

II. EXPERIMENTAL DETAILS

Ta thin films were deposited on SiO_2/Si substrates using a DC magnetron sputtering method; details of deposition and the characteristics from x-ray diffraction and atomic force microscopy measurements were reported previously [22]. Sputtered Ta thin films with a thickness less than 5 nm showed an amorphous structure, and their spatial roughness was measured to be approximately 0.1 nm. The exceptionally low roughness is generally attributed to the favorable wetting property of Ta thin films on SiO_2. The surface roughness of Ta thin films is comparable to those of 2D crystalline superconductors, such as ion-gated ZrNCl [14], whereas much lower than that of highly disordered InOx [11,30]. Table I lists the Ta thin films reported in this paper. The Ta1-1, Ta1-2, and Ta1-3 films were fabricated from the same batch whereas the Ta2-1 film was sputtered from another batch. Film thickness (d) was monitored by a calibrated thickness monitor with a quartz microbalance. Normal state sheet resistance (R_N) is the sheet resistance (R) near 10 K, and T_C is selected when $R = 0.5R_N$. Despite the same nominal thickness, Ta1-2 and Ta2-1 films showed rather dissimilar R_N and accordingly different T_C. We found the film morphologies to vary from batch to batch depending on the details of the fabrication conditions. Nevertheless, Ta films showed consistent transport characteristics within the samples deposited during the same sputtering operation as indicated by batch number. The R_N for the films from the same batch showed a gradual increase with decreasing film thickness.

The Ta films were patterned into four-probe geometries for measurement using a shadow mask during sputtering or electron-beam lithography with a subsequent dry-etching process after sputtering. The transport characteristics were measured by a standard lock-in technique with a measurement frequency of 7–15 Hz and an excitation current of 0.1–10 nA.

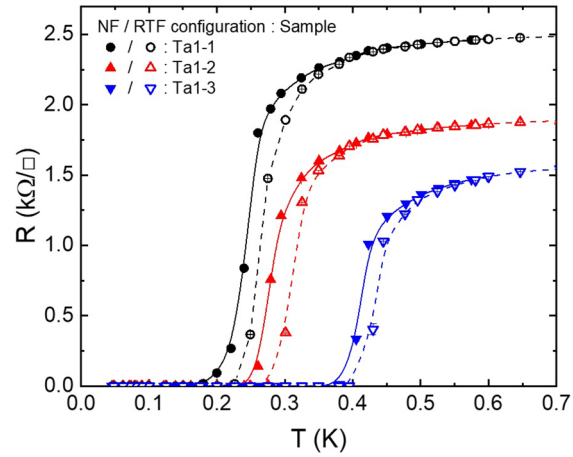

FIG. 1. Temperature dependence of the sheet resistance at zero magnetic field for Ta1-1 (black), Ta1-2 (red), and Ta1-3 (blue). Solid and open symbols show $R(T)$ in the NF and RTF configurations, respectively. The solid and dashed curves are eye guides.

A dilution refrigerator with a superconducting magnet was used to measure the low-temperature characteristics, and a magnetic field perpendicular to the sample plane was applied to study magnetic-field dependence. To investigate the radiation filtering effects, three different configurations were used (see Supplemental Material Fig. S1 [31]). Initially, all samples were measured in a configuration with no low-pass filter [no filter (NF) configuration]. Then, a room-temperature filter (RTF) was installed outside the refrigerator before the measurement lock-in amplifiers (RTF configuration). The RTF consisted of a homemade resistor-capicitor (RC) low-pass filter with a 100-kHz cutoff frequency and a commercial Pi filter with a 10-MHz cutoff frequency. Lastly, in combination with the RTF configuration, an additional low-temperature filter (LTF), comprising RC low-pass filters, was installed in the mixing-chamber stage (R + LTF configuration).

III. RESULTS AND DISCUSSION

Low-temperature transport characteristics were initially investigated to examine the effect of the RTF. The measurement wires were properly heat sunk at all stages of the dilution refrigerator. Figure 1 shows the temperature dependence of the sheet resistance of the Ta thin films with (open symbols) and without (solid symbols) the RTF at zero magnetic field. The T_C values with the RTF are 0.27, 0.32, and 0.44 K for Ta1-1, Ta1-2, and Ta1-3, respectively. As expected, T_C gradually decreased with increasing R_N.

Elimination of the RTF lowered the T_C for all three samples by approximately 25 mK compared to those measured with the RTF. This indicates that typical measurement setups without a RTF cannot successfully prevent the permeation of RF noise down to the sample stage. Such an extensive effect from a single RTF suggests the extreme susceptibility of the superconducting thin films to external perturbations. Similarly, additional dissipation near T_C was reported in 2H-$NbSe_2$ upon the removal of filters, whereas the temperature dependence showed deviation far below T_C in highly disordered amorphous InOx [17]. The marked discrepancy between InOx

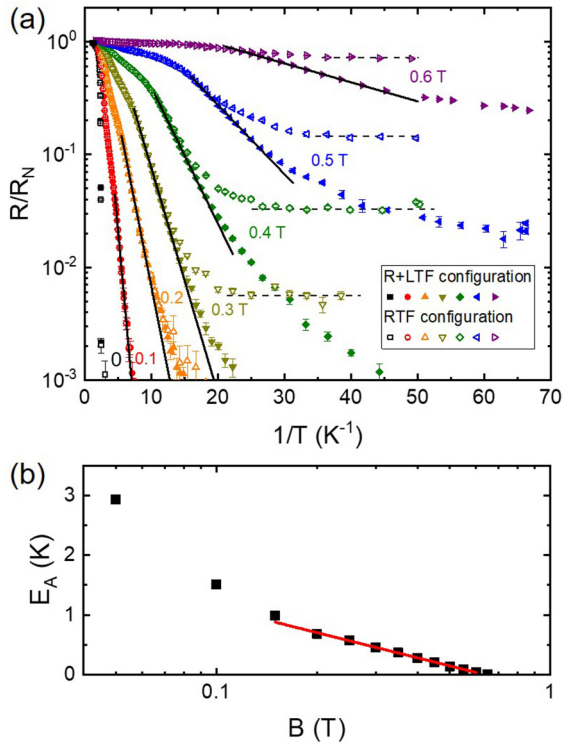

FIG. 2. Temperature dependence of R/R_N under various magnetic fields for Ta2-1. (a) Arrhenius plots under various magnetic fields between 0 and 0.6 T with a 0.1-T step. Solid and open symbols are measured data in the R + LTF and RTF configurations, respectively. Black solid lines are the results of a linear fitting to $R/R_N \propto \exp(-E_A/T)$ with the slopes of the lines representing E_A. Black dashed lines show the saturation of R/R_N to finite values. (b) Magnetic-field dependence of E_A shown in a semilogarithmic plot. The red solid line is a linear fit to $E_A \propto \ln(B_0/B)$ where $B_0 = 0.64$ T.

and 2H-$NbSe_2$ could be ascribed to their film morphologies where the robust percolated superconducting islands in the InOx films are less affected by thermal fluctuations. In other words, the local T_C of superconducting islands exceeds the average mean-field value of the thin film. In the present paper, installation of the RTF did not induce any noticeable change in temperature dependence when the superconducting Ta thin films exhibited zero-resistance superconductivity far below T_C, suggesting that fully developed superconducting thin films are immune (or, at least, less susceptible) to additional thermal fluctuation, similar to the superconducting islands in InOx. Because the zero-resistance state in the RTF configuration appears to be robust, the possible impact of an additional LTF was not emphasized previously [22].

Next, we investigated the effect of the LTF on the transport characteristics. Although the effect of the LTF is not distinct at zero magnetic field, it can be important when the magnetic-field-induced resistive state appears. The temperature dependence of the normalized resistance (R/R_N) of Ta2-1 under various finite magnetic fields below the critical field (B_C) was investigated as shown in Fig. 2(a). The temperature dependence of Ta2-1 with only RTF in an Arrhenius plot (open symbols) reproduced the intriguing intermediate metallic phase within a wide range of magnetic fields. For instance, R/R_N at $B = 0.4$ T exhibits a sharp drop at high temperatures, and the slope in an Arrhenius plot decreases gradually before saturation to a finite value at the zero-temperature limit, which has been regarded as a deviation from the conventional superconducting and insulating states. One can find more pronounced metallic behaviors in the measurements with the NF configuration as shown in Fig. S2 (see the Supplemental Material [31]).

The low-temperature transport properties of the measurements in the R + LTF configuration [Fig. 2(a)] were directly compared with those without the additional LTF. The temperature dependence measured at a magnetic field lower than 0.2 T, which shows a relatively sharp decrease in R/R_N, demonstrates no apparent discrepancy between the two different configurations. At $B \geqslant 0.3$ T, essentially identical temperature dependence between the two configurations is observed at high temperatures where both configurations exhibit thermally activated behaviors. Additional filtering exerts a discernible influence at low-resistance regions where the sheet resistance drops to approximately 2% of R_N at $B = 0.3$ T. The intensively filtered film still follows the thermally activated behavior [see, e.g., solid black lines in Fig. 2(a)] whereas the conventionally filtered film deviates from it. Further decreasing temperature reveals that R/R_N of the intensively filtered film can have two orders of magnitude smaller R/R_N than that of the film without the LTF at sufficiently low temperatures. Besides, the installation of the LTF destroys the finite-resistance saturation as shown with the dashed lines, which has been considered to be a hallmark of the quantum metallic phase. It is notable that the R/R_N of the thin film with the LTF eventually deviates from the black solid line and subsequently further decreases to a lower value without obvious saturation. One may attempt to explain this deviation via the extreme susceptibility of 2D superconducting films to external perturbations, even though the effect is now extremely minute. However, we cannot exclude the possibility of the quantum metallic state existing in a very narrow range of magnetic fields near the quantum critical point.

Thermally activated behavior at intermediate temperatures can be characterized by a simple equation, $R/R_N \propto \exp(-E_A/T)$ where the activation energy E_A, the slope of the black line, is typically an average energy barrier for trapped vortices. Figure 2(b) shows the magnetic-field dependence of E_A. The red solid line illustrates the logarithmic dependence of E_A on the magnetic field, i.e., $E_A \propto \ln(B_0/B)$ where $B_0 = 0.64$ T. This logarithmic dependence is understood by the thermal activation energy barrier required for generating a free dislocation-antidislocation pair [10,32].

We also observed distinct filtering effects in magnetoresistance (MR) isotherm measurements. Figure 3(a) shows MR isotherm curves for Ta2-1 measured at various temperatures in the R+ LTF configuration. Representative MR characteristics near the critical point $B_C \approx 0.65$ T, where dR/dT changes its sign were reproduced. The MR isotherm curves show steeper declines at lower temperature with uniform magnetic-field dependence, where R/R_N follows $\exp(B/B^*)$. One may recognize that the MR changes the slope at a certain magnetic field where the dominant vortex dynamics may be altered with increasing vortex density. One may also speculate that the extreme susceptibility of 2D superconducting films at

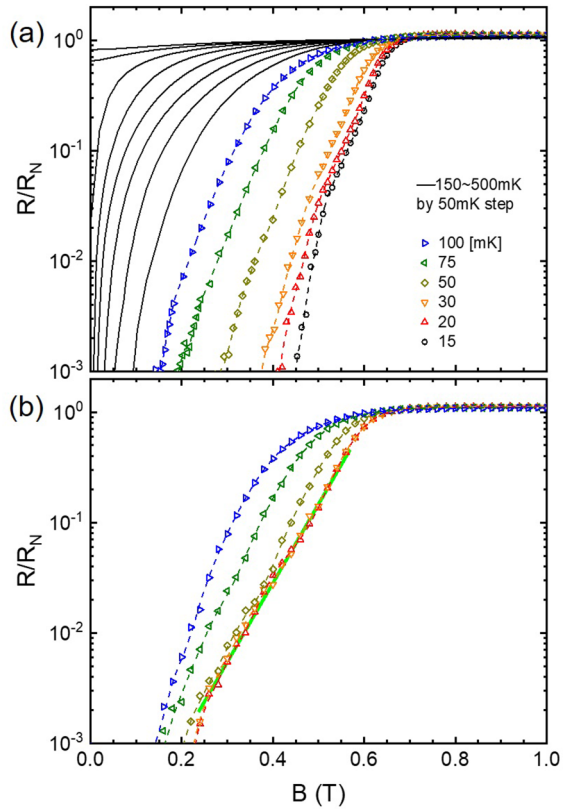

FIG. 3. MR isotherms at various temperatures. (a) R/R_N of Ta2-1 as a function of magnetic field measured in the R + LTF configuration. Black solid lines are measured at various temperatures between 150 and 500 mK with a 50-mK step. The data points with different colors are measured at $T = 100$ (▷), 75 (◁), 50 (◇), 30 (▽), 20 (△), and 15 (◯) mK, respectively, and the dashed lines are eye guides. (b) Magnetic-field dependence of R/R_N in the RTF configuration. The data points are measured at $T = 100$, 75, 50, 30, and 20 mK, and the dashed lines are eye guides. The measurement temperatures are displayed in the same colors and symbols as those in (a). The green solid line exhibits the exponential dependence of $R \sim \exp(B/B^*)$.

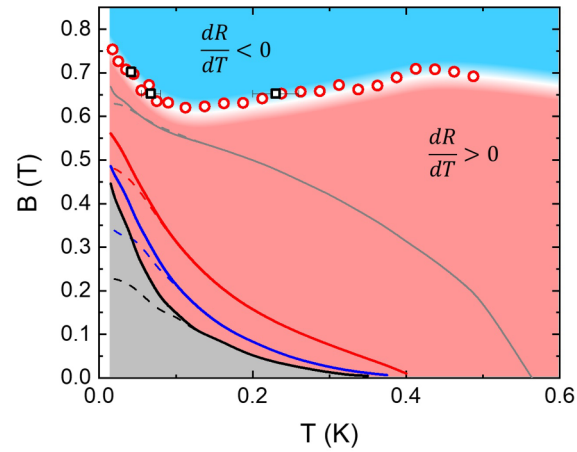

FIG. 4. Transport phase diagram of Ta2-1 on the B-T plane constructed from measurements in the R + LTF configuration except for the dashed lines. The red open circles, B_{Cross}, are the crossing points of two adjacent MR isotherms [Fig. 3(a)], and the black open squares, T_{Cross}, are the crossover points between negative and positive dR/dT, obtained from the $R(T)$ curves under 0.65 and 0.7 T (see Fig. S3 in the Supplemental Material [31]). The blue- and red-shaded regions show negative and positive dR/dT, respectively. The gray-shaded area indicates the zero-resistance region in our measurement limit. Gray, red, blue, and black solid lines are isodissipative curves of $0.9R_N$, $0.1R_N$, $0.01R_N$, and $0.001R_N$ in the R + LTF configuration, respectively. The dashed lines (gray, red, blue, and black) are isodissipative curves ($0.9R_N$, $0.1R_N$, $0.01R_N$, and $0.001R_N$) obtained from measurements in the RTF configuration.

low temperatures may eventually affect the magnetic-field dependence.

The most striking observation is that the MR curves with the additional LTF do not overlap with other isotherms even near the base temperature below 20 mK, demonstrating that no saturated finite resistance at low temperatures is present. On the contrary, MR isotherm curves less than 30 mK overlap well with a single curve in the measurements without the LTF, which is consistent with the appearance of the saturated resistance at low temperatures with finite magnetic field [see Fig. 2(a)]. The collapsed MR isotherms show a single exponential field dependence of $R/R_N \propto \exp(B/B^*)$ as marked by a green solid line in Fig. 3(b). In the MR isotherms measured at $T \geqslant 50$ mK, distinct separation from the collapsed isotherms is observed. For instance, the MR isotherm at $T = 50$ mK initially follows the collapsed isotherms and then branches off near 0.4 T. With further increasing temperature, isotherm curves at $T \geqslant 75$ mK are separated from the low-temperature behavior at all magnetic-field ranges. The exponential magnetic-field dependence of saturated resistance and the dissociation of high-temperature MR isotherms are compatible with previously reported MR measurements of amorphous MoGe [23].

The temperature and magnetic-field dependencies demonstrate that the magnetic-field-induced metallic behavior in a Ta thin film can be vastly reduced with intensive filtering. The crucial role of the LTF can be additionally understood by examining the phase diagram of the Ta thin film on the B-T plane; Fig. 4 displays a reconstructed phase diagram based on the transport measurements in the R + LTF configuration shown in Figs. 2(a) and 3(a). B_{Cross} (red open circles) obtained from Fig. 3(a) is the crossing point between two adjacent MR isotherm curves, indicating that the Ta film at $B > B_{\mathrm{Cross}}$ exhibits insulating behavior at the zero-temperature limit. The boundary connecting B_{Cross} points separates the insulating phase from the superconducting (or metallic) phase. Additionally, direct measurements of the sheet resistance as a function of temperature in the very narrow range of magnetic fields near B_C reveal the crossing points T_{Cross} where the sign of dR/dT is reversed. T_{Cross} values are obtained by temperature-dependence measurements at $B = 0.65$ and 0.7 T (see Fig. S3 in the Supplemental Material [31]) and plotted with black open squares in the diagram. The crossing points show excellent agreement with the SI phase boundary as shown in Fig. 4.

The SI transition at the zero-temperature limit can be understood within the framework of the quantum melting of the vortex lattice. The phase boundary between a superconductor and an insulator near the quantum critical point is expected to have relatively weak temperature dependence. However, B_{Cross} in the phase diagram (Fig. 4) exhibits a

steep increase with decreasing temperature below 0.1 K, suggesting that the destruction of the superconducting phase is further complicated by the interplay of quantum fluctuations, thermal fluctuations, and disorders in the thin film. The low-temperature upturn of B_{Cross} is remarkably similar to that observed in 3-ML Ga films [33] where the presence of quenched disorders stabilized the local vortex glasslike phases in the epitaxially grown atomically thin films. Accordingly, "global" superconductivity can be induced at extremely low temperatures by long-range Josephson coupling of the superconducting islands. We speculate that the temperature dependence of B_{Cross} in the Ta thin films with relatively weak disorders can be understood with essentially the same framework as the vortex glasslike state at low temperatures.

In Fig. 4, the blue-shaded area above the phase boundary, which is determined by the red open circles and the black open squares, shows the negative dR/dT region, whereas the red-shaded area indicates the positive dR/dT region. The temperature dependence of the sheet resistance in the positive dR/dT region is clarified further by isoresistive curves of $0.9R_N$, $0.1R_N$, $0.01R_N$, and $0.001R_N$. The dashed lines with the same colors represent the transport measurements in the RTF configuration with corresponding values of the sheet resistance to compare with the intensively filtered results. All solid lines show steep increases, consistently below about 0.1 K. Similarly, the zero-resistance region in our measurement limit (gray area) increases sharply, nearly identical to the metal-insulator boundary. On the other hand, measurements with only the RTF (dashed lines) show resistance saturation because of thermal broadening at low temperatures, which leads to the elusive appearance of the metallic phase. At the base temperature of our dilution refrigerator, the zero-resistance region is defined below approximately 0.45 T and extrapolated to 0.55 T at the zero-temperature limit. Therefore, the intrinsic metallic ground state, if it exists, is expected to be only in a narrow range of magnetic fields near B_C.

The reduction of the metallic phase with intensive filtering indicates that Ta thin films can be as sensitive as 2D crystalline 2H-$NbSe_2$ to external perturbations. Ta thin films with thickness less than 5 nm are microscopically disordered, similar to amorphous InOx films. However, the surface roughness in Ta films is an order of magnitude smaller than that of InOx films. We speculate that the vortices are pinned rather weakly in a Ta thin film due to its surface morphology with low vortex pinning barriers. Weakly pinned vortices can be agitated by small perturbations easily and moved with resistive dissipation, which leads to a broadening of the transition with finite-resistance saturation even below 0.1 K. This seems consistent with the extreme sensitivity of the vortex state in amorphous MoGe films to external RF radiation [34]. Presumably, an appropriate filtering of electromagnetic radiation results in a dramatic suppression of the mobility of vortices. In addition, because electron-phonon scattering in 2D superconducting films near zero temperature becomes extremely weak, thin films could be extremely susceptive to even small external radiation. Although Ta films are disordered, the exceedingly low T_C compared to that of typical InOx films may allow one to measure the marked difference.

However, the reduction of thermal fluctuations with extensive filtering is not sufficient to eliminate the metallic phase completely. Deviation from thermally activated dependence was entirely eliminated with the installation of an LTF in Ref. [17]; in the present paper though, the low-temperature deviation is still present in the Ta thin film. Non-Arrhenius temperature dependence of $\exp[-(E_0/T)^p]$ with $p < 1$ (see short-dotted lines in Supplemental Material Fig. S4 [31]) was obtained in a disordered InOx film [11], which could be ascribed to variable-range-hopping resistivity induced by quantum vortex tunneling [35]. Otherwise, continuous changes in the dominant thermally activated mechanism with decreasing temperature are another possible explanation to understand the deviation [32]. Dissipation in a vortex lattice arises due to the phase fluctuations mediated by the displacements of dislocations, which have two temperature-dependent terms: the rate of thermally activated dislocation creep over the pinning barriers and the density of thermally activated free dislocation pairs. In the weak collective pinning region where the interaction energy of the vortices is more significant than the characteristic pinning barrier of disorders, resistance mainly depends on the density of thermally activated dislocations at sufficiently high temperatures, which can explain the logarithmic magnetic-field dependence of E_A shown in Fig. 2(b). At low temperatures, when only disorder-induced dislocations remain, the main temperature-dependence term is the thermal creep rate of the surviving dislocations, which will appear as thermally activated dependence with another characteristic activation energy from the pinning barriers.

To summarize, we studied the effect of radiation on the metallic phase in superconducting Ta films with three different filtering configurations (NF, RTF, and R + LTF). A significantly reduced metallic phase was obtained in the transport measurements with the R + LTF configuration, demonstrating that the unfiltered, thermally agitated fluctuations are mainly responsible for the elusive metallic phase. Since the thermally activated process with decreasing temperature was not fully recovered with intensive filtering, there could be other possible explanations for the low-temperature transport properties in Ta thin films. To clarify the temperature dependence at low temperatures, it is necessary to investigate electron temperature in the different filtering configurations.

ACKNOWLEDGMENTS

This work was supported by the National Research Foundation of Korea (NRF) Grant funded by the Korean Government (MSIP) (NRF-2016R1A5A1008184) and the MSIT (Ministry of Science and ICT), Korea, under the ITRC (Information Technology Research Center) support program (IITP-2020-2018-0-01402) supervised by the IITP (Institute for Information & Communications Technology Planning & Evaluation).

[1] E. Abrahams, P. W. Anderson, D. C. Licciardello, and T. V. Ramakrishnan, Phys. Rev. Lett. **42**, 673 (1979).

[2] M. P. A. Fisher, Phys. Rev. Lett. **65**, 923 (1990).

[3] A. M. Finkel'stein, Physica B **197**, 636 (1994).

[4] S. L. Sondhi, S. M. Girvin, J. P. Carini, and D. Shahar, Rev. Mod. Phys. **69**, 315 (1997).
[5] A. F. Hebard and M. A. Paalanen, Phys. Rev. Lett. **65**, 927 (1990).
[6] D. B. Haviland, Y. Liu, and A. M. Goldman, Phys. Rev. Lett. **62**, 2180 (1989).
[7] R. Crane, N. P. Armitage, A. Johansson, G. Sambandamurthy, D. Shahar, and G. Grüner, Phys. Rev. B **75**, 184530 (2007).
[8] B. Sacépé, C. Chapelier, T. I. Baturina, V. M. Vinokur, M. R. Baklanov, and M. Sanquer, Phys. Rev. Lett. **101**, 157006 (2008).
[9] P. Spathis, H. Aubin, A. Pourret, and K. Behnia, Europhys. Lett. **83**, 57005 (2008).
[10] D. Ephron, A. Yazdani, A. Kapitulnik, and M. R. Beasley, Phys. Rev. Lett. **76**, 1529 (1996).
[11] I. M. Percher, I. Volotsenko, A. Frydman, B. I. Shklovskii, and A. M. Goldman, Phys. Rev. B **96**, 224511 (2017).
[12] Y. Qin, C. L. Vicente, and J. Yoon, Phys. Rev. B **73**, 100505(R) (2006).
[13] A. W. Tsen, B. Hunt, Y. D. Kim, Z. J. Yuan, S. Jia, R. J. Cava, J. Hone, P. Kim, C. R. Dean, and A. N. Pasupathy, Nat. Phys. **12**, 208 (2016).
[14] Y. Saito, Y. Kasahara, J. Ye, Y. Iwasa, and T. Nojima, Science **350**, 409 (2015).
[15] P. Phillips and D. Dalidovich, Science **302**, 243 (2003).
[16] E. Shimshoni, A. Auerbach, and A. Kapitulnik, Phys. Rev. Lett. **80**, 3352 (1998).
[17] I. Tamir, A. Benyamini, E. J. Telford, F. Gorniaczyk, A. Doron, T. Levinson, D. Wang, F. Gay, B. Sacépé, J. Hone, K. Watanabe, T. Taniguchi, C. R. Dean, A. N. Pasupathy, and D. Shahar, Sci. Adv. **5**, eaau3826 (2019).
[18] C. Yang, Y. Liu, Y. Wang, L. Feng, Q. He, J. Sun, Y. Tang, C. Wu, J. Xiong, W. Zhang, X. Lin, H. Yao, H. Liu, G. Fernandes, J. Xu, J. M. Valles, J. Wang, and Y. Li, Science **366**, 1505 (2019).
[19] P. W. Phillips, Science **366**, 1450 (2019).
[20] Y. Seo, Y. Qin, C. L. Vicente, K. S. Choi, and J. Yoon, Phys. Rev. Lett. **97**, 057005 (2006).
[21] Y. Li, C. L. Vicente, and J. Yoon, Phys. Rev. B **81**, 020505(R) (2010).
[22] S. Park, J. Shin, and E. Kim, Sci. Rep. **7**, 42969 (2017).
[23] N. Mason and A. Kapitulnik, Phys. Rev. B **64**, 060504(R) (2001).
[24] N. Mason and A. Kapitulnik, Phys. Rev. Lett. **82**, 5341 (1999).
[25] A. Benyamini, E. J. Telford, D. M. Kennes, D. Wang, A. Williams, K. Watanabe, T. Taniguchi, D. Shahar, J. Hone, C. R. Dean, A. J. Millis, and A. N. Pasupathy, Nat. Phys. **15**, 947 (2019).
[26] Y. Xing, K. Zhao, P. Shan, F. Zheng, Y. Zhang, H. Fu, Y. Liu, M. Tian, C. Xi, H. Liu, J. Feng, X. Lin, S. Ji, X. Chen, Q. K. Xue, and J. Wang, Nano Lett. **17**, 6802 (2017).
[27] G. Sambandamurthy, L. W. Engel, A. Johansson, and D. Shahar, Phys. Rev. Lett. **92**, 107005 (2004).
[28] M. Steiner and A. Kapitulnik, Physica C **422**, 16 (2005).
[29] G. Kopnov, O. Cohen, M. Ovadia, K. H. Lee, C. C. Wong, and D. Shahar, Phys. Rev. Lett. **109**, 167002 (2012).
[30] K. H. S. B. Tan, K. A. Parendo, and A. M. Goldman, Phys. Rev. B **78**, 014506 (2008).
[31] See Supplemental Material at http://link.aps.org/supplemental/10.1103/PhysRevB.102.184501 for schematics of measurement configurations, additional experimental data, and analyses.
[32] M. V. Feigel'man, V. B. Geshkenbein, and A. I. Larkin, Physica C **167**, 177 (1990).
[33] Y. Xing, H.-M. Zhang, H.-L. Fu, H. Liu, Y. Sun, J.-P. Peng, F. Wang, X. Lin, X.-C. Ma, Q.-K. Xue, J. Wang, and X. C. Xie, Science **350**, 542 (2015).
[34] S. Dutta, I. Roy, S. Mandal, J. Jesudasan, V. Bagwe, and P. Raychaudhuri, Phys. Rev. B **100**, 214518 (2019).
[35] M. P. A. Fisher, T. A. Tokuyasu, and A. P. Young, Phys. Rev. Lett. **66**, 2931 (1991).